Imperial College London

Imperial College London

Department of Electrical and Electronic Engineering

Signal Optimization for Wireless Information and Power Transmission

Author:
Yang Zhao
(CID: 01561245)

Supervisor:
Dr Bruno Clerckx

Co-Supervisor:
Dr Morteza Varasteh

A thesis submitted for the degree of

MSc Communications and Signal Processing

August 18, 2019

Contents

List of Figures

List of Tables

Chapter 1

Introduction

1.1 Literature Review

Battery has become a main power source for most mobile devices. However, limited operation time and high cost in recharging or replacement have become bottlenecks for smart networks as Internet-of-Things (IoT). As a promising solution, Energy Harvesting (EH) from the ambient environment can potentially provide perpetual power to the devices. Compared with other renewable resources as solar, wind and water, Radio-Frequency (RF) waves typically contain less energy and are more suitable for low-power applications as Wireless Sensor Network (WSN). Recently, the significant reduction in power requirements of chips and processors brings more attention to Wireless Power Transfer (WPT) in both academia and industry [1, 2, 3, 4, 5, 6, 7, 8, 9, 10].

On the other hand, RF radiation has been a medium for Wireless Information Transfer (WIT) for more than a century. Naturally, a unified design of Wireless Information and Power transmission (WIPT) is expected to be a prominent solution to power billions of mobile devices while keeping them connected. [1] first defined a nonlinear concave capacity-energy function and investigated the tradeoff for typical binary channels and a flat additive white Gaussian noise (AWGN) channel with amplitude-constrained inputs. It was extended to frequency-selective channel in [2]. However, both works were based on the impractical assumption that information decoding (ID) and EH can be performed individually on the same received signal. In [3], the authors proposed two practical co-located receiver designs named *time switching* (TS) that switches between ID and EH and *power splitting* (PS) that splits the received power into two separate streams. It was then demonstrated in [11] that TS can guarantee the same rate as conventional Time-Division Multiple Access (TDMA) while providing considerable power. In comparison, PS may lead to higher rate when the demand on power is sufficiently high. A further research [12] enabled dynamic power splitting that adjusts the power split ratio based on the channel state information (CSI), and proposed a suboptimal low-complexity *antenna switching* scheme. Nevertheless, the literatures above are mostly based on an oversimplified linear harvester model. To accurately characterize the behavior of the rectenna, [13] derived a tractable nonlinear model and performed an adaptive multisine waveform design accordingly. Realistic simulations showed significant gains in harvested power and stressed the importance of modelling rectifier nonlinearity in wireless system design. The work was extended to multi-input single-output

(MISO) WIPT in [14] where a superposition of multicarrier modulated and unmodulated waveform was optimized as a function of CSI under transmit power budget. It suggested the rectifier nonlinearity can lead to a larger rate-energy (R-E) region and favours a different waveform, modulation and input distribution. In another perspective, a learning approach [15] modelled the transmitter and receiver as deep neural networks (NN) and jointly optimized signal encoding with network parameters. Constellations showed that the offset of the power symbol is positively correlated to the power demand, while the information symbols are symmetrically located around the origin. The pattern confirmed a unmodulated waveform is beneficial to increase the harvested power in [14].

Chapter 2

From WPT to WIPT

In this section, we first introduce a general WPT architecture. Next, we focus on the rectenna behavior and derive the analytical diode models for the energy harvester. We then extend the work to WIPT and explore two practical receiver structures. Finally, the signal and system model is established, and the dependency of delivered power on signal design is investigated on top of it.

2.1 WPT Architecture

According to the operation principle, WPT systems can be categorized as *maximum power transfer* that maximizes the coverage and *maximum energy efficiency transfer* [4] that compromise with the power budget. Figure 2.1 illustrates the fundamental blocks of a generic WPT system.

The transmit power efficiency e is decomposed as:

$$e = \frac{P_{\mathrm{dc,ST}}}{P_{\mathrm{dc}}^t} = \underbrace{\frac{P_{\mathrm{rf}}^t}{P_{\mathrm{dc}}^t}}_{e_1} \cdot \underbrace{\frac{P_{\mathrm{rf}}^r}{P_{\mathrm{rf}}^t}}_{e_2} \cdot \underbrace{\frac{P_{\mathrm{dc}}^r}{P_{\mathrm{rf}}^r}}_{e_3} \cdot \underbrace{\frac{P_{\mathrm{dc,ST}}}{P_{\mathrm{dc}}^r}}_{e_4} \tag{2.1}$$

Most existing solutions assumed no dependency for the components and focused on maximizing each term individually. Nevertheless, it has been proved by [7, 13, 16] that these efficiencies are indeed coupled with each other, especially when input power is low (below 1 mW). Specifically, the DC-to-RF efficiency e_1 is related to the Peak-to-Average Power Ratio (PAPR) hence the waveform [17]. Similarly, the RF-to-RF efficiency e_2 is determined by the channel state and the signal characteristics as waveform, beamformer, modulation, and power allocation [18]. It also desires a highly directional transmission [19]. e_3 measures the RF-to-DC efficiency of the rectenna, which relates to the rectifier input power P_{rf}^r [20, 21, 10], channel and the
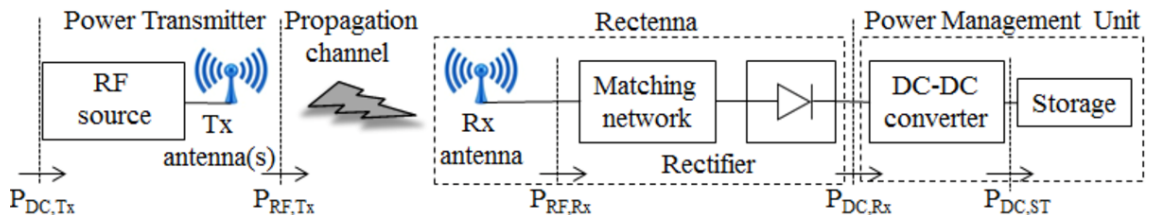

Figure 2.1: Block diagram of a conventional far-field WPT architecture [10]

transmit signal [22, 23, 18]. Finally, the DC-to-DC efficiency e_4 can be maximized by dynamically adjusting the rectifier load with the diode impedance [24]. Therefore, we desire a flexible transmitter to optimize the signal adaptively over CSI to maximize the power transfer efficiency e.

From the perspective of WPT, this article particularly investigates the relationship between signal design and $e_2 \cdot e_3$ based on the nonlinear harvester model proposed in [13].

2.2 Rectenna Design

2.2.1 Rectenna Behavior

A rectenna receives electromagnetic power with antenna and convert it to electric power with rectifier. Diverse configurations are available for energy harvesting, such as *Schottky* [25, 26], *CMOS* [27, 6], *series* [28, 29], *shunt* [30, 31]. Interestingly, those models are not equally suitable for the same input power, and maximizing the rectenna efficiency e_3 requires a proper selection according to the power range. As reported in [6, 9], low barrier Schottky diodes are commonly used for input power between $1\,\mu W$ and $1\,mW$. Specifically, single diode is preferred for low power below $500\,\mu W$ and multiple diodes are typically applied for input power above $500\,\mu W$ [18]. Hybrid designs as [32] may be employed to maintain a high efficiency for large power range.

Besides the rectenna model, the shape of the received signal also influences the RF-to-DC efficiency e_3. It was first demonstrated in [20] that multisine waveform *i.e. Power-Optimized waveform (POW)* outperforms the single tone waveform *i.e. Continuous Wave (CW)* in operation range and power efficiency. The expression of a multisine waveform with N subcarriers writes as a summation of N sine waves:

$$V_{\text{multisine}}(t) = \sum_{n=0}^{N-1} \frac{1}{\sqrt{N}} \sin\left(2\pi\left(f_0 + n\Delta f\right)t\right) \tag{2.2}$$

where f_0 is the minimum frequency and Δf is the spacing. Figure 2.2 [20] illustrates the three-subcarrier case for both signals in time and frequency domains. It can be observed that multisine waveform provides a higher PAPR equals to $\sqrt{N}$ and occupies a bandwidth of $(N-1)\Delta f$ with the same average power as CW, which is equally distributed to its components.

The advantage of multisine in WPT is that the high PAPR increases the peak rectifier output voltage. With a proper signal and circuit design, high voltage may be preserved during the cycle if discharging is slow enough, as indicated by the thick blue line in Figure 2.2b. To enhance the harvested power, a large number of tones may be used to increase PAPR, and the multisine signal will appear as pulses with period of $1/\Delta f$. Most of the signal power will be concentrated in those pulses to trigger the diode and charge the capacitor. However, more subbands can lead to smaller frequency gaps and longer charging cycle when the bandwidth is fixed.

It can be hard to derive an accurate expression of the RF-to-DC efficiency e_3 on the power and shape of the rectifier input signal, as practical energy harvesting circuits consists of various nonlinear components as diodes, capacitors and inductors.
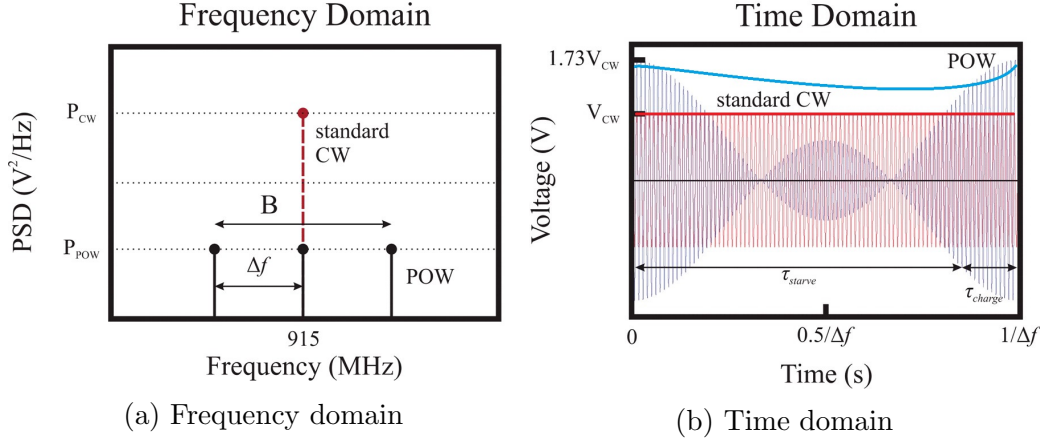
(a) Frequency domain

(b) Time domain

Figure 2.2: Comparison of a typical 3-subcarrier multisine and CW in time and frequency domains (modified from [20]). The thick lines are examples of rectifier output voltage.

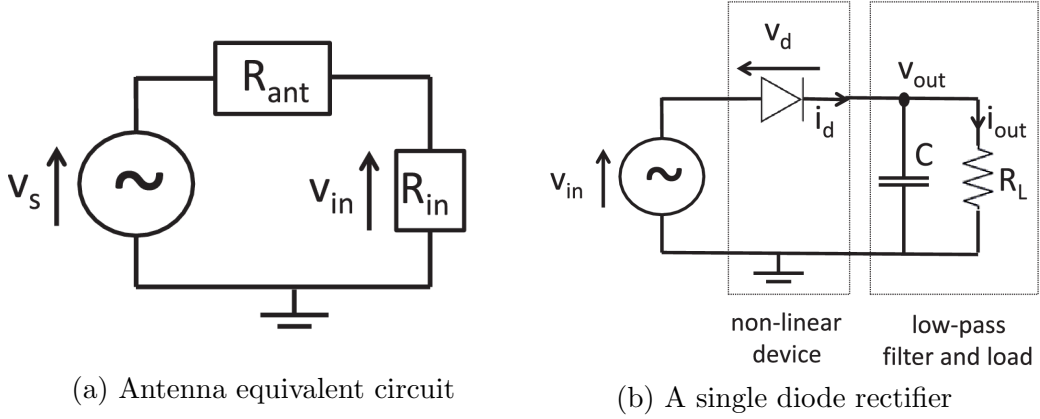(a) Antenna equivalent circuit

(b) A single diode rectifier

Figure 2.3: Rectenna architecture

It is also sensitive to parasitic sources, impedance matching, and harmonic generation [33, 6]. In this article, we employ the *diode linear model* and *diode nonlinear model* proposed in [13] based on the diode current-voltage (I-V) characteristics to capture the fundamental pattern of rectenna and investigate its impact on resource allocation and system design. A superposed waveform containing modulated information and multisine power components is optimized according to CSI on top of both models.

2.2.2 Antenna Model

As illustrated by Figure 2.3b, the rectifier consists of a single diode as the source of nonlinearity and a low-pass filter to store energy.

Figure 2.3a shows that the antenna equivalent circuit includes a voltage source $v_s(t)$ connected to a series antenna impedance $Z_{ant} = R_{ant} + jX_{ant}$ followed by a combined impedance of the rectifier and the matching network $Z_{in} = R_{in} + jX_{in}$. Assuming lossless, the perfect matching condition is

$$R_{in} = R_{ant}, X_{in} = -X_{ant} \tag{2.3}$$

When equation 2.3 is satisfied, the rectifier input voltage equals

$$v_{\text{in}}(t) = v_{\text{s}}(t)/2 = y(t)\sqrt{R_{\text{in}}} \tag{2.4}$$

where $y(t)$ is the received signal. Therefore, the input power to the rectifier writes

$$P_{\text{rf}}^{r} = \mathbb{E}\left[y(t)^2\right] = \mathbb{E}\left[v_{\text{in}}(t)^2\right]/R_{\text{in}} \tag{2.5}$$

It is also assumed that the noise is too small to be harvested.

2.3 Diode Linear and Nonlinear Models

Consider the single diode rectifier presented in Figure 2.3b for simplicity. Without loss of generality, the employed diode models hold for general circuits as voltage doubler and bridge rectifiers [34].

Denote $v_{\text{in}}(t)$ and $v_{\text{out}}(t)$ as diode input and output voltages, the voltage across the diode is $v_{\text{d}}(t) = v_{\text{in}}(t) - v_{\text{out}}(t)$. It determines the current flowing through the diode:

$$i_{\text{d}}(t) = i_{\text{s}}\left(e^{\frac{v_{\text{d}}(t)}{nv_{\text{t}}}} - 1\right) \tag{2.6}$$

where i_{s} is the reverse saturation current, n is the ideality factor, and v_{t} is the thermal voltage. With a Taylor series expansion around a quiescent point $a = v_{\text{d}}(t)$, equation 2.6 rewrites as:

$$i_{\text{d}}(t) = \sum_{i=0}^{\infty} k_i'(v_{\text{d}}(t) - a)^i \tag{2.7}$$

where

$$k_i' = \begin{cases} i_{\text{s}}\left(e^{\frac{a}{nv_{\text{t}}}} - 1\right), & i = 0 \\ i_{\text{s}}\dfrac{e^{\frac{a}{nv_{\text{t}}}}}{i!(nv_{\text{t}})^i}, & i \in \mathbb{N}^+ \end{cases} \tag{2.8}$$

k_i' relates to the diode parameters and is a constant when a is fixed. Note that the Taylor series expression is a small-signal model that only fits for the nonlinear operation region of the diode. Therefore, equation 2.7 is no longer accurate for a large input voltage $v_{\text{in}}(t)$, where the diode behavior is dominated by the series resistor and the I-V relationship is linear [26].

Also, we assume an ideal rectifier with steady-state response that delivers a constant output voltage v_{out}, whose amplitude is only a function of the peaks of the input voltage $v_{\text{in}}(t)$ [35]. Based on the assumptions, a proper choice of voltage drop would be

$$a = \mathbb{E}\left[v_{\text{d}}(t)\right] = \mathbb{E}\left[v_{\text{in}}(t) - v_{\text{out}}\right] = -v_{\text{out}} \tag{2.9}$$

as

$$\mathbb{E}\left[v_{\text{in}}(t)\right] = \sqrt{R_{\text{ant}}}\mathbb{E}\left[y(t)\right] = 0 \tag{2.10}$$

9

On top of equation 2.9 and 2.4, the diode current in 2.7 can be expressed as

$$i_{\mathrm{d}}(t) = \sum_{i=0}^{\infty} k_i' v_{\mathrm{in}}(t)^i = \sum_{i=0}^{\infty} k_i' R_{\mathrm{ant}}^{i/2} y(t)^i \tag{2.11}$$

Equation 2.11 reveals an explicit relationship between the received waveform $y(t)$ and the diode current $i_{\mathrm{d}}(t)$. Nevertheless, as the signal carries both power and information simultaneously, the waveform varies at every symbol period due to the randomness of modulation. Hence, the diode current $i_{\mathrm{d}}(t)$ fluctuates with time as well. By taking an expectation over the symbol distribution, the harvested DC current can be modelled as

$$i_{\mathrm{out}} = \mathbb{E}\left[i_{\mathrm{d}}(t)\right] \tag{2.12}$$

and the available power is

$$P_{\mathrm{dc}}^r = i_{\mathrm{out}}^2 R_{\mathrm{L}} \tag{2.13}$$

To investigate the fundamental dependency of harvested power on waveform design, a practical strategy is to approximate equation 2.11 with a truncation to the n_o-th order:

$$i_{\mathrm{out}} \approx \sum_{i=0}^{n_o} k_i' R_{\mathrm{ant}}^{i/2} \mathbb{E}\left[y(t)^i\right] \tag{2.14}$$

The contribution of odd terms is indeed zero, as $\mathbb{E}\left[y(t)^i\right] = 0$ for odd i. Therefore, we only need to model the even terms:

$$i_{\mathrm{out}} \approx \sum_{i \text{ even}}^{n_o} k_i' R_{\mathrm{ant}}^{i/2} \mathbb{E}\left[y(t)^i\right] \tag{2.15}$$

2.4 Receiver Architectures

We investigated two practical architectures for the co-located integrated information and energy receiver. Both designs are equipped with individual ID and EH receivers. The former is a conventional baseband demodulator while the latter can be realized with the proposed rectifier structure in Section 2.2.

2.4.1 Time Switching

A *Time Switching (TS)* receiver (Figure 2.4) operates as either an information decoder or an energy harvester at a certain time. In the design, the transmitter divides the transmission block into orthogonal power and data slots with length ratio α and $1 - \alpha$ respectively, then optimizes the waveform for WIT or WPT individually. Also, the receiver periodically switches between ID and EH receivers in the corresponding slots. We assume perfect synchronization between transmitter and receiver for mode control. It can achieve different rate-energy tradeoffs by adjusting the slot length ratio α jointly with the transmit signals. As the input power range for information and power receivers are typically different, TS can be combined with a "near-far" scheduling [3] to benefit the system efficiency.
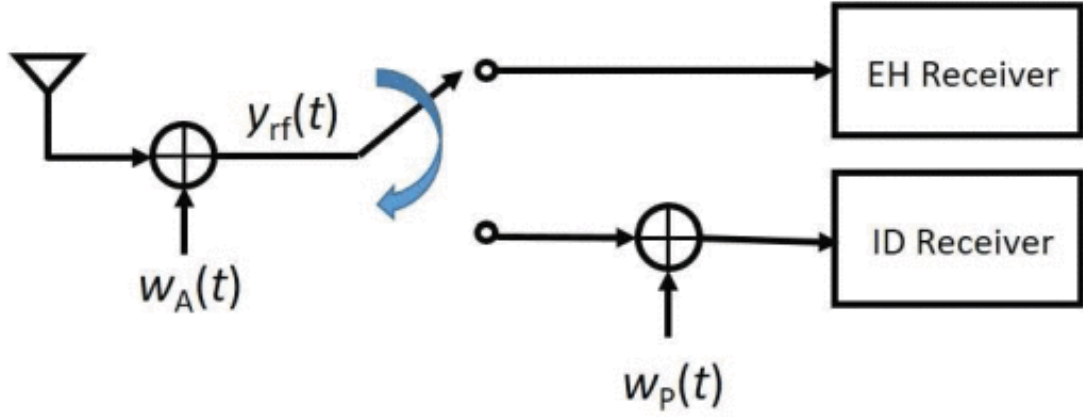
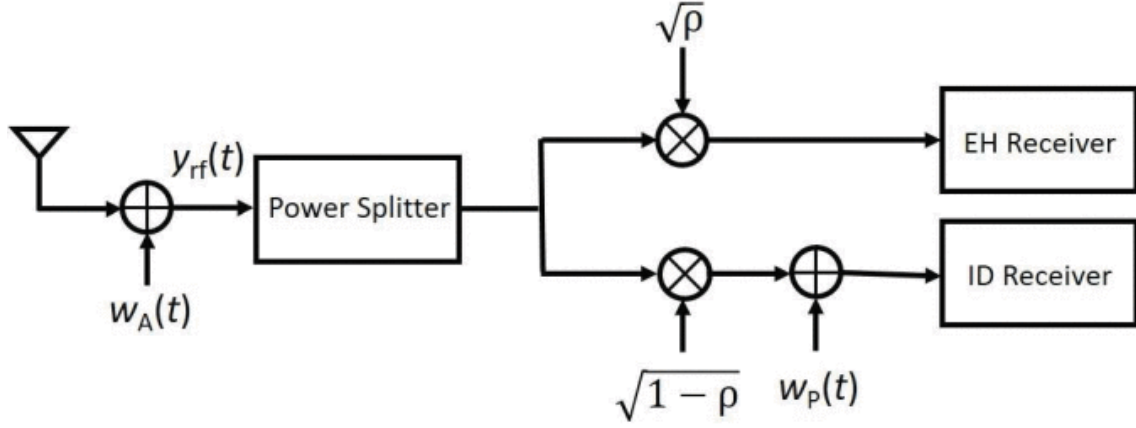Figure 2.4: Structure of time switching receiver [18]

Figure 2.5: Structure of power splitting receiver [18]

2.4.2 Power Splitting

In a *Power Splitting (PS)* receiver (Figure 2.5), we introduce a PS ratio ρ to split the received signal into separate power stream (with proportion ρ) and information stream (with proportion $1 - \rho$). At the transmitter, the signal is jointly optimized for information and power transmission according to CSIT. With the assumption of perfect matching, the EH and ID receivers are with input voltage signals $\sqrt{\rho R_{\text{ant}}} y(t)$ and $\sqrt{(1 - \rho) R_{\text{ant}}} y(t)$ respectively. Varying the PS ratio ρ and the transmit signals leads to different rate-energy points. It is argued in [3] that the PS scheme is optimal for ideal RF-to-baseband signal conversion with negligible processing noise, but the condition is hard to meet in practice.

2.5 Signal and System Model

Consider a point-to-point MISO WIPT system in multipath environment. The M-antenna transmitter delivers information and power simultaneously to the single-antenna receiver through N orthogonal subbands. It is assumed the carrier frequencies are with even spacing Δf and equal bandwidth B_{s}. The n-th subband has carrier frequency $f_n = f_0 + n \Delta f$ for $n = 0, \ldots, N - 1$. To maximize the rate-energy

tradeoff, we employ a superposed signal consists of a multi-carrier deterministic multisine waveform and a multi-carrier random modulated waveform for power and information delivery respectively. Both components are transmitted on the same frequency bands.

2.5.1 Transmitted Information Waveform

Denote the information symbol carried by the modulated waveform on subband n as $\tilde{x}_n$, we assume the input symbol is with the capacity-achieving i.i.d. Circular Symmetric Complex Gaussian (CSCG) distribution with zero mean and unit variance [36]:

$$\tilde{x}_n = |\tilde{x}_n| e^{j\phi_{\tilde{x}_n}} \sim \mathcal{CN}(0,1) \tag{2.16}$$

Hence, the modulated waveform on antenna $m = 1, \ldots, M$, subband n writes as

$$x_{n,m} = w_{I,n,m} \tilde{x}_n \tag{2.17}$$

where $w_{I,n,m}$ is the corresponding information weight and is a constant for a certain channel state:

$$w_{I,n,m} = |w_{I,n,m}| e^{j\phi_{I,n,m}} = s_{I,n,m} e^{j\phi_{I,n,m}} \tag{2.18}$$

Note the amplitude and phase are separated in resource allocation. Define matrices $\mathbf{S}_I$ and $\mathbf{\Phi}_I$ of size $N \times M$ such that the (n, m) entries hold $s_{I,n,m}$ and $\phi_{I,n,m}$ respectively, the design of information waveform is converted into an optimization problem on both matrices, with the average WIT transmit power $P_I = \frac{1}{2} \|\mathbf{S}_I\|_F^2$. The modulated symbol of equation 2.17 can be further expressed as

$$x_{n,m} = s_{I,n,m} e^{j\phi_{I,n,m}} \cdot |\tilde{x}_n| e^{j\phi_{\tilde{x}_n}} = \tilde{s}_{I,n,m} e^{j\tilde{\phi}_{I,n,m}} \tag{2.19}$$

with $\tilde{s}_{I,n,m} = s_{I,n,m} |\tilde{x}_n|$ and $\tilde{\phi}_{I,n,m} = \phi_{I,n,m} + \phi_{\tilde{x}_n}$. In this way, the impact of symbol distribution and waveform design are combined. The modulated waveform also follows an i.i.d. CSCG distribution with variance equal to the subband power $x_{n,m} \sim \mathcal{CN}\left(0, s_{I,n,m}^2\right)$.

Therefore, the information waveform $x_{I,m}(t)$ on antenna m at time t writes as

$$x_{I,m}(t) = \sum_{n=0}^{N-1} \tilde{s}_{I,n,m}(t) \cos\left(2\pi f_n t + \tilde{\phi}_{I,n,m}(t)\right) \tag{2.20}$$

$$= \Re\left\{\sum_{n=0}^{N-1} x_{n,m}(t) e^{j2\pi f_n t}\right\} \tag{2.21}$$

$$= \Re\left\{\sum_{n=0}^{N-1} w_{I,n,m} \tilde{x}_n(t) e^{j2\pi f_n t}\right\} \tag{2.22}$$

On top of this, the WIT signal vector is spread over M antennas

$$\mathbf{x}_I(t) = \Re\left\{\sum_{n=0}^{N-1} \mathbf{w}_{I,n} \tilde{x}_n(t) e^{j2\pi f_n t}\right\} \tag{2.23}$$

where $\mathbf{w}_{I,n} = [w_{I,n,1} \cdots w_{I,n,M}]^T$.

2.5.2 Transmitted Power Waveform

Comparing with the information component, the multisine power component is unmodulated and deterministic, so there is no dependency on the distribution of input symbol $\tilde{x}_n(t)$. The power waveform on antenna m, subband n is given by

$$w_{P,n,m} = s_{P,n,m}e^{j\phi_{P,n,m}} \tag{2.24}$$

where $s_{P,n,m}$ and $\phi_{P,n,m}$ are the amplitude and phase of the multisine signal. Collect them into the (n,m) entries of matrices $\mathbf{S}_P$ and $\mathbf{\Phi}_P$, the average power of the WPT waveform is $\frac{1}{2}\|\mathbf{S}_P\|_F^2$. Similarly, the power waveform $x_{P,m}(t)$ on antenna m at time t is

$$x_{P,m}(t) = \sum_{n=0}^{N-1} s_{P,n,m}\cos\left(2\pi f_n t + \phi_{P,n,m}\right) \tag{2.25}$$

$$= \Re\left\{\sum_{n=0}^{N-1} w_{P,n,m}e^{j2\pi f_n t}\right\} \tag{2.26}$$

Combine the power signals on all M antennas, the WPT signal vector writes as

$$\mathbf{x}_P(t) = \Re\left\{\sum_{n=0}^{N-1} \mathbf{w}_{P,n}e^{j2\pi f_n t}\right\} \tag{2.27}$$

with $\mathbf{w}_{P,n} = [w_{P,n,1}\cdots w_{P,n,M}]^T$.

2.5.3 Multipath Channel and Received Signal

Consider a multipath channel with L paths. For the l-th path $(l = 1,\ldots,L)$, denote the phase shift between the receive antenna and transmit antenna m of subband n as $\zeta_{n,m,l}$. Let τ_l and α_l be the delay and magnitude gain, and indicate the transmit signal on subband n of antenna m as

$$v_{n,m}(t) = w_{P,n,m} + w_{I,n,m}\tilde{x}_n(t) \tag{2.28}$$

The superposed signal containing modulated information waveform and multisine power waveform is demonstrated to bring a two-fold benefit on rate and energy [18]. Also, the channel frequency response is expressed as

$$h_{n,m} = \sum_{l=0}^{L-1} \alpha_l e^{j\left(-2\pi f_n\tau_l + \zeta_{n,m,l}\right)} \tag{2.29}$$

To ensure $v_{n,m}(t)$ and $\tilde{x}_n(t)$ being narrowband signals, we assume $\max_{l\neq l'}|\tau_l - \tau_{l'}| << 1/B_s$. It is also supposed that $v_{n,m}(t - \tau_l) = v_{n,m}(t)$ and $\tilde{x}_n(t - \tau_l) = \tilde{x}_n(t)$. The received signal corresponding to transmit antenna m contains the power component $y_{P,m}(t)$ and the information component $y_{I,m}(t)$

$$y_m(t) = y_{P,m}(t) + y_{I,m}(t) \tag{2.30}$$

$$= \Re \left\{ \sum_{l=0}^{L-1} \sum_{n=0}^{N-1} \alpha_l v_{n,m} (t - \tau_l) e^{j2\pi f_n(t-\tau_l)+\zeta_{n,m,l}} \right\} \tag{2.31}$$

$$\approx \Re \left\{ \sum_{n=0}^{N-1} h_{n,m} v_{n,m}(t) e^{j2\pi f_n t} \right\} \tag{2.32}$$

Hence, the total received signal can be obtained by stacking up equation 2.30 over all transmit signals

$$\mathbf{y}(t) = \mathbf{y}_P(t) + \mathbf{y}_I(t) \tag{2.33}$$

$$= \Re \left\{ \sum_{n=0}^{N-1} \mathbf{h}_n \left(\mathbf{w}_{P,n} + \mathbf{w}_{I,n} \tilde{x}_n \right) e^{j2\pi f_n t} \right\} \tag{2.34}$$

where the channel vector is defined as $\mathbf{h}_n = [h_{n,1} \dots h_{n,M}]$.

2.6   Information Decoder

In the superposed transmit signal $x_m(t)$, the modulated component $x_{I,m}(t)$ carries all the information while the multisine component $x_{P,m}(t)$ completely serves the power. Since the latter is deterministic, it creates no interference and has zero contribution to the different entropy of $x_m(t)$ in terms of translation. Therefore, the achievable rate is equal to

$$I\left(\mathbf{S}_I, \mathbf{\Phi}_I, \rho\right) = \sum_{n=0}^{N-1} \log_2 \left(1 + \frac{(1-\rho)|\mathbf{h}_n \mathbf{w}_{I,n}|^2}{\sigma_n^2} \right) \tag{2.35}$$

where σ_n^2 is the total variance of the Gaussian noise at the RF-band and the noise introduced during the RF-to-baseband conversion (assumed Gaussian) on tone n. It achieves the maximum rate $I\left(\mathbf{S}_I^\star, \mathbf{\Phi}_I^\star, 0\right)$ and boils down to WIT by setting $\rho = 0$ then performing Maximum Ratio Transmission (MRT) and Water-Filling (WF) power allocation on subbands.

An significant conclusion in [14] is that the rate 2.35 is always achievable with and without waveform cancellation. As the multisine is deterministic, it can either be subtracted from the baseband signal or used to construct the translated codebook. Conventional demodulation can be performed then.

Bibliography

[1] B. Clerckx, A. Costanzo, A. Georgiadis, and N. Borges Carvalho, "Toward 1G Mobile Power Networks: RF, Signal, and System Designs to Make Smart Objects Autonomous," *IEEE Microwave Magazine*, vol. 19, no. 6, pp. 69–82, 2018.

[2] M. S. Trotter, J. D. Griffin, and G. D. Durgin, "Power-optimized waveforms for improving the range and reliability of RFID systems," *2009 IEEE International Conference on RFID, RFID 2009*, pp. 80–87, 2009.

[3] B. Clerckx, R. Zhang, R. Schober, D. W. K. Ng, D. I. Kim, and H. V. Poor, "Fundamentals of wireless information and power transfer: From RF energy harvester models to signal and system designs," *IEEE Journal on Selected Areas in Communications*, vol. 37, no. 1, pp. 4–33, 2019.

[4] L. R. Varshney, "Transporting Information and Energy Simultaneously," *IEEE International Symposium on Information Theory - Proceedings*, pp. 1612–1616, 2008.

[5] P. Grover and A. Sahai, "Shannon meets tesla: Wireless information and power transfer," *IEEE International Symposium on Information Theory - Proceedings*, pp. 2363–2367, 2010.

[6] R. Zhang and C. K. Ho, "MIMO broadcasting for simultaneous wireless information and power transfer," *IEEE Transactions on Wireless Communications*, vol. 12, no. 5, pp. 1989–2001, 2013.

[7] S. Y. Hui, W. Zhong, and C. K. Lee, "A critical review of recent progress in mid-range wireless power transfer," *IEEE Transactions on Power Electronics*, vol. 29, no. 9, pp. 4500–4511, 2014.

[8] I. Krikidis, S. Timotheou, S. Nikolaou, G. Zheng, D. W. K. Ng, and R. Schober, "Simultaneous Wireless Information and Power Transfer in modern communication systems," *IEEE Communications Magazine*, vol. 52, no. 11, pp. 104–110, 2014.

[9] C. R. Valenta and G. D. Durgin, "Harvesting wireless power: Survey of energy-harvester conversion efficiency in far-field, wireless power transfer systems," *IEEE Microwave Magazine*, vol. 15, no. 4, pp. 108–120, 2014.

[10] E. Boshkovska, D. W. K. Ng, N. Zlatanov, and R. Schober, "Practical non-linear energy harvesting model and resource allocation for SWIPT systems," *IEEE Communications Letters*, vol. 19, no. 12, pp. 2082–2085, 2015.

[11] Z. Ding, C. Zhong, D. Wing Kwan Ng, M. Peng, H. A. Suraweera, R. Schober, and H. V. Poor, "Application of smart antenna technologies in simultaneous wireless information and power transfer," *IEEE Communications Magazine*, vol. 53, no. 4, pp. 86–93, 2015.

[12] A. Costanzo and D. Masotti, "Smart Solutions in Smart Spaces: Getting the Most from Far-Field Wireless Power Transfer," *IEEE Microwave Magazine*, vol. 17, no. 5, pp. 30–45, 2016.

[13] X. Zhou, R. Zhang, and C. K. Ho, "Wireless information and power transfer in multiuser OFDM systems," *GLOBECOM - IEEE Global Telecommunications Conference*, vol. 13, no. 4, pp. 4092–4097, 2013.

[14] L. Liu, R. Zhang, and K. C. Chua, "Wireless information and power transfer: A dynamic power splitting approach," *IEEE Transactions on Communications*, vol. 61, no. 9, pp. 3990–4001, 2013.

[15] B. Clerckx and E. Bayguzina, "Waveform Design for Wireless Power Transfer," *IEEE Transactions on Signal Processing*, vol. 64, no. 23, pp. 6313–6328, 2016.

[16] B. Clerckx, "Wireless Information and Power Transfer: Nonlinearity, Waveform Design, and Rate-Energy Tradeoff," *IEEE Transactions on Signal Processing*, vol. 66, no. 4, pp. 847–862, 2018.

[17] M. Varasteh, E. Piovano, and B. Clerckx, "A Learning Approach To Wireless Information and Power Transfer Signal and System Design," pp. 4534–4538, 2018. [Online]. Available: http://arxiv.org/abs/1810.12152

[18] Y. Zeng, B. Clerckx, and R. Zhang, "Communications and Signals Design for Wireless Power Transmission," *IEEE Transactions on Communications*, vol. 65, no. 5, pp. 2264–2290, 2017.

[19] A. S. Boaventura and N. B. Carvalho, "Maximizing DC power in energy harvesting circuits using multisine excitation," *IEEE MTT-S International Microwave Symposium Digest*, vol. 1, no. 1, pp. 1–4, 2011.

[20] T. Takahashi, T. Mizuno, M. Sawa, T. Sasaki, T. Takahashi, and N. Shinohara, "Development of phased array for high accurate microwave power transmission," *2011 IEEE MTT-S International Microwave Workshop Series on Innovative Wireless Power Transmission: Technologies, Systems, and Applications, IMWS-IWPT 2011 - Proceedings*, pp. 157–160, 2011.

[21] Y. S. Chen and C. W. Chiu, "Maximum achievable power conversion efficiency obtained through an optimized rectenna structure for RF energy harvesting," *IEEE Transactions on Antennas and Propagation*, vol. 65, no. 5, pp. 2305–2317, 2017.

[22] A. Collado and A. Georgiadis, "Optimal waveforms for efficient wireless power transmission," *IEEE Microwave and Wireless Components Letters*, vol. 24, no. 5, pp. 354–356, 2014.

[23] A. Boaventura, D. Belo, R. Fernandes, A. Collado, A. Georgiadis, and N. B. Carvalho, "Boosting the Efficiency: Unconventional Waveform Design for Efficient Wireless Power Transfer," *IEEE Microwave Magazine*, vol. 16, no. 3, pp. 87–96, 2015.

[24] A. Dolgov, R. Zane, and Z. Popovic, "Power management system for online low power RF energy harvesting optimization," *IEEE Transactions on Circuits and Systems I: Regular Papers*, vol. 57, no. 7, pp. 1802–1811, 2010.

[25] J. A. G. Akkermans, M. C. Van Beurden, G. J. N. Doodeman, and H. J. Visser, "Analytical models for low-power rectenna design," *IEEE Antennas and Wireless Propagation Letters*, vol. 4, no. 1, pp. 187–190, 2005.

[26] A. Boaventura, A. Collado, N. B. Carvalho, and A. Georgiadis, "Optimum behavior: Wireless power transmission system design through behavioral models and efficient synthesis techniques," *IEEE Microwave Magazine*, vol. 14, no. 2, pp. 26–35, 2013.

[27] M. Stoopman, S. Keyrouz, H. J. Visser, K. Philips, and W. A. Serdijn, "Co-design of a CMOS rectifier and small loop antenna for highly sensitive RF energy harvesters," *IEEE Journal of Solid-State Circuits*, vol. 49, no. 3, pp. 622–634, 2014.

[28] A. Georgiadis, A. Collado, S. Via, and C. Meneses, "Flexible hybrid solar/EM energy harvester for autonomous sensors," *IEEE MTT-S International Microwave Symposium Digest*, pp. 1–4, 2011.

[29] A. Collado and A. Georgiadis, "Conformal hybrid solar and electromagnetic (EM) energy harvesting rectenna," *IEEE Transactions on Circuits and Systems I: Regular Papers*, vol. 60, no. 8, pp. 2225–2234, 2013.

[30] J. O. McSpadden, L. Fan, and K. Chang, "Design and Experiments of a High-Conversion-Efficiency 5.8-GHz Rectenna," *IEEE Transactions on Microwave Theory and Techniques*, vol. 46, no. 12, pp. 2053–2060, 1998.

[31] J. Guo and X. Zhu, "An improved analytical model for RF-DC conversion efficiency in microwave rectifiers," *IEEE MTT-S International Microwave Symposium Digest*, pp. 1–3, 2012.

[32] H. Sun, Z. Zhong, and Y. X. Guo, "An adaptive reconfigurable rectifier for wireless power transmission," *IEEE Microwave and Wireless Components Letters*, vol. 23, no. 9, pp. 492–494, 2013.

[33] B. Strassner and K. Chang, "Microwave power transmission: Historical milestones and system components," *Proceedings of the IEEE*, vol. 101, no. 6, pp. 1379–1396, 2013.

[34] B. Clerckx and E. Bayguzina, "Low-Complexity Adaptive Multisine Waveform Design for Wireless Power Transfer," *IEEE Antennas and Wireless Propagation Letters*, vol. 16, no. 1, pp. 2207–2210, 2017.

[35] J.-p. Curty, N. Joehl, C. Dehollain, and M. J. Declercq, "A Model for Mu-Power Rectifier Analysis and Design," *Technology*, vol. 52, no. 12, pp. 2771–2779, 2005. [Online]. Available: http://scholar.google.com/scholar?hl=en{&}btnG=Search{&}q=intitle: A+Model+for+-Power+Rectifier+Analysis+and+Design{#}0

[36] M. Varasteh, B. Rassouli, and B. Clerckx, "On Capacity-Achieving Distributions for Complex AWGN Channels Under Nonlinear Power Constraints and their Applications to SWIPT," vol. 2017, 2017. [Online]. Available: http://arxiv.org/abs/1712.01226